RESEARCH ARTICLE

Editor's Choice

ADVANCED MATERIALS TECHNOLOGIES

www.advmattechnol.de

Accessible Soft Electronics with Silver-Gelatin Conductive Hydrogel Composite

*Kiyn Chin, Michael Vinciguerra, Dinesh K. Patel, Peter Roberts Olcay, Eldy S. Lazaro Vasquez, and Carmel Majidi**

Electrically conductive hydrogels are a promising class of materials for soft electronics and robotics that mimic the mechanics of natural biological tissue. However, these materials are typically derived from petrochemical sources and their production typically involves hazardous solvents and monomers that limit accessibility and environmental compatibility. This study introduces a biomaterial hydrogel composite in which a percolating network of silver microflakes is suspended in a natural, gelatin-based matrix. The composite is primarily composed of inexpensive, food-safe ingredients and fabrication is achieved using accessible consumer-grade equipment. The resulting material system is mechanically soft, stretchable up to 470% strain, and highly conductive up to 3.1 × 10^3 S cm^{-1}, with properties that can be tailored based on material composition and processing conditions. In addition to experimental characterization of its material properties, this conductive gelatin composite is shown to be applicable for a variety of uses cases in soft matter circuitry and bioelectronics.

1. Introduction

Natural materials derived from renewable biological sources have the potential to replace materials extracted from petroleum byproducts or other non-renewable sources for use in next generation soft machines and electronics.[1–4] Gelatin (denatured animal collagen) is especially promising since it can be engineered to exhibit mechanical properties similar to synthetically-derived soft elastomers and gels while also being sourced from agricultural waste, avoiding new environmental exploitation.[5,6] Given these potential benefits in the face of growing climate instability,[7] work is underway to incorporate gelatin and other sustainable and food-grade materials into emerging technological applications, including soft circuity and bioelectronics.[8]

A versatile approach to creating materials from gelatin is as the polymer in a hydrogel, a composite material composed of a polymer matrix swollen with an interstitial aqueous phase. Gelatin-based hydrogels and their conductive composites have been of particular interest for their versatility in creating structures and devices.[9] There exists an intrinsic tension between mechanical and electrical properties for deformable conductors,[10] so tunability is of great importance. The accessibility, biodegradability and mechanical tunability of gelatin has been established by Baumgartner et al., with additional demonstration of integration into soft circuitry and robotics.[11] 3D printability of optically clear gelatin for use in waveguides for sensing and as the bulk structure of a soft mechanism was demonstrated by Heiden et al.[12] A functional soft robotic pneumatic actuator using a gelatin-glycerol hydrogel structure has been demonstrated by Shintake et al.,[13] and Matonis et al. fabricated fully edible origami-inspired actuators from genipin-crosslinked gelatin.[14] Hardman et al. showed ionically conductive gelatin-glycerol hydrogel for strain sensing.[15] Jing et al. created a conductive filled composite from thiolated gelatin with silver nanowires(GE-SH-AgNWs), designed for wearable strain sensing.[16] Liu et al. showed a gelatin hydrogel soaked in ammonium sulfate forming an ionically conductive hydrogel.[17] Park et al. used reduced graphene oxide (rGO) as a conductive filler in methacrylated (GelMA) gelatin to form conductive hydrogel (r(GO/GelMA)) for applications as a nerve conduit.[18] Han et al. combined dopamine grafted gelatin with graphene oxide as conductive filler to form a self-healing, adhesive hydrogel.[19]

There have been several simple fabrication processes leveraged in the formation of conductive hydrogels that are promising for accessible fabrication processes. The "salt-out" effect was leveraged using baths of sodium sulfate or ammonium sulfate

K. Chin, M. Vinciguerra, D. K. Patel, P. Roberts Olcay, C. Majidi
Department of Mechanical Engineering
Carnegie Mellon University
Pittsburgh, PA 15213, USA
E-mail: cmajidi@andrew.cmu.edu

K. Chin, C. Majidi
The Robotics Institute
Carnegie Mellon University
Pittsburgh, PA 15213, USA

E. S. L. Vasquez
ATLAS Institute
University of Colorado Boulder
Boulder, CO 80309, USA

The ORCID identification number(s) for the author(s) of this article can be found under https://doi.org/10.1002/admt.202401193

DOI: 10.1002/admt.202401193

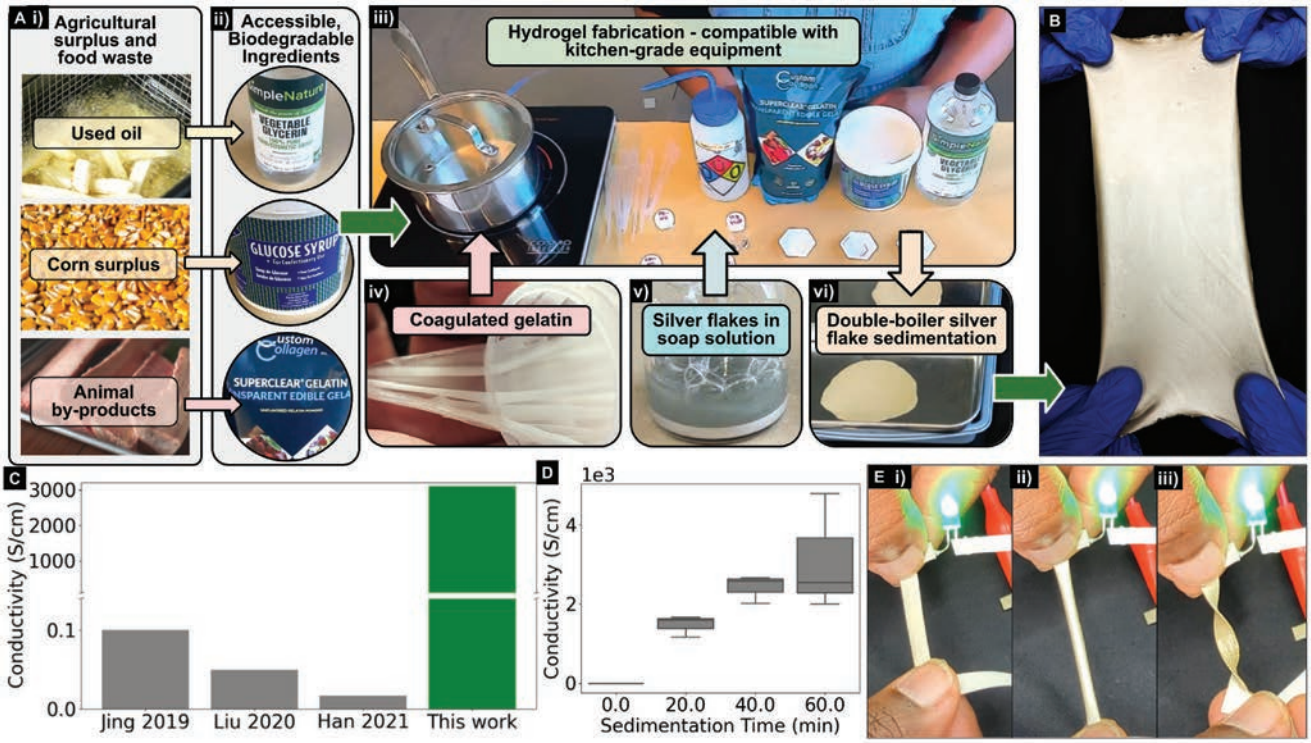

Figure 1. A) Accessible naturally-derived ingredients and inexpensive equipment for the fabrication of conductive hydrogel composite. Images in i) adapted with permission (by Ron Lach, José Roberto Oliveira, and Los Muertos Crew respectively, via Pexels) B) Stretched sheet of conductive gelatin sample. C) Comparison of conductivity of this work conductive coagulated gelatin (CG-C) to conductive gelatin composites in literature.[16,17,19] D) Electrical conductivity of CG-C conductive gelatin increasing as a function of sedimentation time. E) Strip of conductive glycerol-rich gelatin (GG-C) sample functioning as a wire in a circuit under 1) normal conditions, 2) stretching, and 3) torsion.

after the synthesis of the base hydrogel.[16,17,20] Ohm et al. showed that partial dehydration of a silver–polyacrylamide–alginate hydrogel can increase conductivity by reducing the space between high aspect ratio conductive particles.[21] Zhao et al. showed extremely high conductivities via dry annealing and freeze-thaw processing in a polyvinyl alcohol-Borax hydrogel with silver (Ag) microflakes and gallium-indium alloy liquid metal droplets.[22] Ford et al. observed that sedimentation of liquid metal particles in rubber-hydrogel composite could affect conductivity.[23] Gan et al. demonstrated sedimentation of liquid metal droplets in gelatin gel and subsequent sintering via gel dehydration to produce thin-films with high stretchability and conductivity.[24] Most of these processes produce either highly conductive hydrogels or are created from sustainable ingredient sources, but not both. The work of Gan et al. achieves these goals, at the cost of producing only a thin-film form factor and relying on expensive and low-availability liquid metal conductive filler. An important space remains for a hydrogel produced from sustainable, inexpensive ingredient sources that achieves conductivities over the 10^2 S cm^{-1} threshold for use in a variety of soft matter electronics.

In this work, we introduce an electrically conductive hydrogel composed of silver (Ag) microflakes embedded within a network of food grade materials like gelatin (biopolymer), glucose syrup (cosolvent) and glycerol (cosolvent and plasticizer) (**Figure 1**A). These ingredients are inexpensive due to their ready availability, either derived from animal residues in agricultural waste (gelatin), extracted from plant or animal fats (glycerol), or refined from a wide variety of crops (glucose syrup). Not only are their sources renewable, these ingredients are byproducts and the bulk of their production is driven by co-products with much larger markets: meat or other animal products for gelatin, biofuels for glycerol and subsidized corn and sugar for glucose syrup. Biodiesel production produces a marked excess of glycerol, posing environmental challenges for disposal,[25] and the excess of high-fructose corn syrup (glucose syrup) resulting from subsidies has been identified as a driver of public health decline in the United States.[26] By introducing value-added uses for these materials and providing an outlet for existing surplus, the overall sustainability calculus of their sources and co-products can be improved. The fabrication process for producing the composite is designed to be compatible with standard kitchen equipment and can be implemented in a well-ventilated domestic environment (Figure 1 Aiii). Together, the choice of inexpensive and consumer-grade materials and equipment make this a relatively *accessible* approach to engineering conductive hydrogel compared to other methods that require access to laboratory-grade chemicals and facilities. To demonstrate the use of the conductive silver-gelatin composite in practical applications, we show that the conductor can be used as a stretchable, finger-mounted electrode that maintains an electrical connection with finger motion and a forearm-mounted bioelectronic sticker that tracks hand motion through electromyography. Collectively, these measurements and demonstrations suggest that silver-gelatin composites could be promising for accessible soft

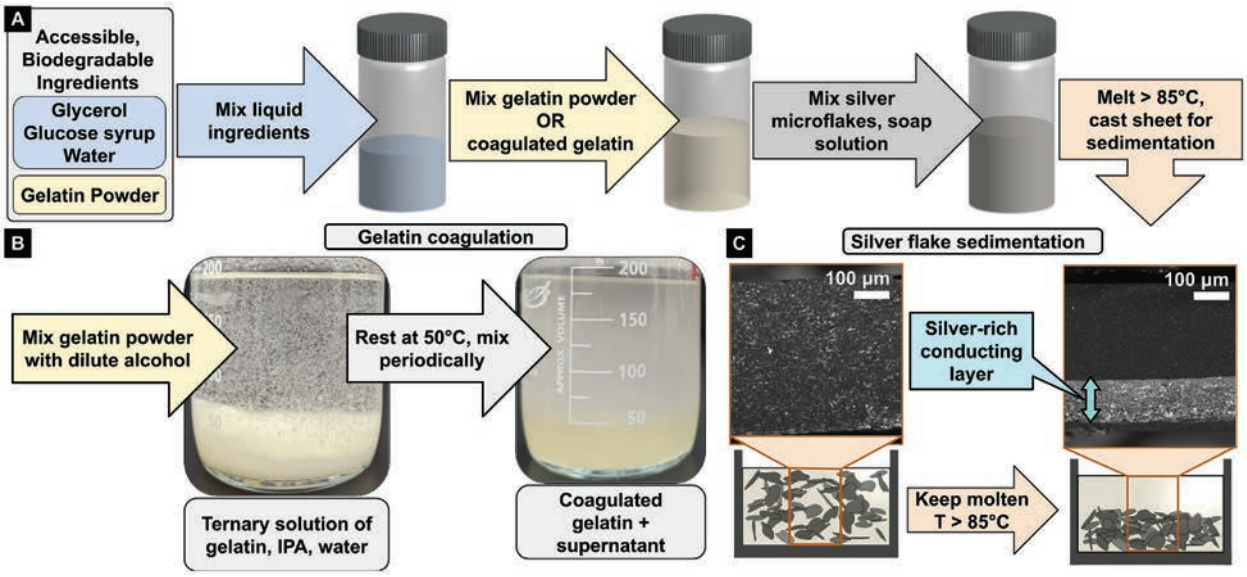

Figure 2. A) Fabrication process of conductive gelatin hydrogel bulk material. B) Process for coagulation of gelatin into longer polymer chains. Isopropyl alcohol (IPA) is a non-solvent of gelatin and is miscible with water, producing a ternary solution with dynamic pairwise molecular interactions that lead to longer condensation polymerization reaction times and thus longer chain lengths. C) Process for gravitational sedimentation of silver microflakes to produce conductive layer. Temperatures above melting point and inclusion of dish soap surfactant allow all silver flakes to progressively sediment to the bottom of the material and form a percolating network.

electronics that can be produced with readily-available materials and resources.

2. Results

In the material system presented here, electrical conductivity is achieved through the use of a common conductive filler, silver microflakes. To reduce the amount of silver required to achieve percolation and electrical conductivity, we exploit a combination of a partial dehydration of the hydrogel matrix as pioneered in Ohm et al.[21] and a novel gravity-driven filler sedimentation strategy. We tailor the mechanical properties of the conductive hydrogel composite through the addition of glucose and glycerol and the coagulation of gelatin biopolymer. Glycerol is used as a plasticizer, while both glycerol and glucose syrup are used as cosolvents, improving the strain-at-break of the material. Localized phase separation due to exclusion of cosolvents from polymer chain surfaces has been proposed as a mechanism for this effect, due to a higher density of reversible/dynamic hydrogen bonds between gelatin helices in the gelatin-rich regions.[11,27] Glycerol acts as a plasticizer, enhancing chain mobility. Gelatin coagulation extends the chain length of gelatin biopolymer,[28] allowing for the formation of dynamic mechanical bonds known as entanglements. Polymer networks with a high number of entanglements have been shown to have high strain-at-break while maintaining elasticity due to the ability to store energy during tension in many entangled chains without breaking bonds.[29,30] We pursue this combination of strategies for enhancing mechanical properties rather than chemically cross-linking the gelatin in order to maintain the thermoplastic properties of temperature-controlled reversible phase change, and the resulting possibility of easily retrieving conductive filler.

The silver-gelatin composite can be produced in a domestic kitchen environment by mixing silver flakes (47MR-10F, Inframat Advanced Materials) with store-bought, food-grade materials – gelatin, glucose syrup, glycerol and water. Details of the complete fabrication process are presented in **Figure 2**, Movies S1–S4 (Supporting Information) and also described in the Experimental Section. As shown in the Figure 2, the glycerol, glucose syrup, and gelatin powder are first mixed with water and then combined with silver microflakes and dish soap solution. The resulting mixture is then poured into a mold or dropcast on a substrate over >85° C in order to maintain a fluidic state and allow the Ag flakes to settle and form a sedimentation layer on the bottom of the material. The dish soap acts as a surfactant, preventing the silver flakes from floating on the surface and forming an electrically disconnected layer on top of the material. Following a prescribed sedimentation time of 20–60 min, the material is allowed to cool and harden to form a hydrogel. Lastly, the silver-gelatin composite can be removed from the mold or substrate. Depending on the Ag flake concentration and settling time, the sedimented side of the composite can exhibit a volumetric electrical conductivity up to 3.1×10^3 S cm^{-1}. The following subsections describe how alterations in gelatin composition and Ag sedimentation time can influence mechanical, electrical, and electromechanical properties of the composite.

2.1. Material Structure and Composition

The hydrogel matrix is composed of gelatin (coagulated or unmodified), glucose syrup, glycerol, and water. The mechanical and electrical properties of the final composite depend on the particular ratios of ingredients and the gelatin type. Rather than a full exploration of this parameter space, we start with a baseline

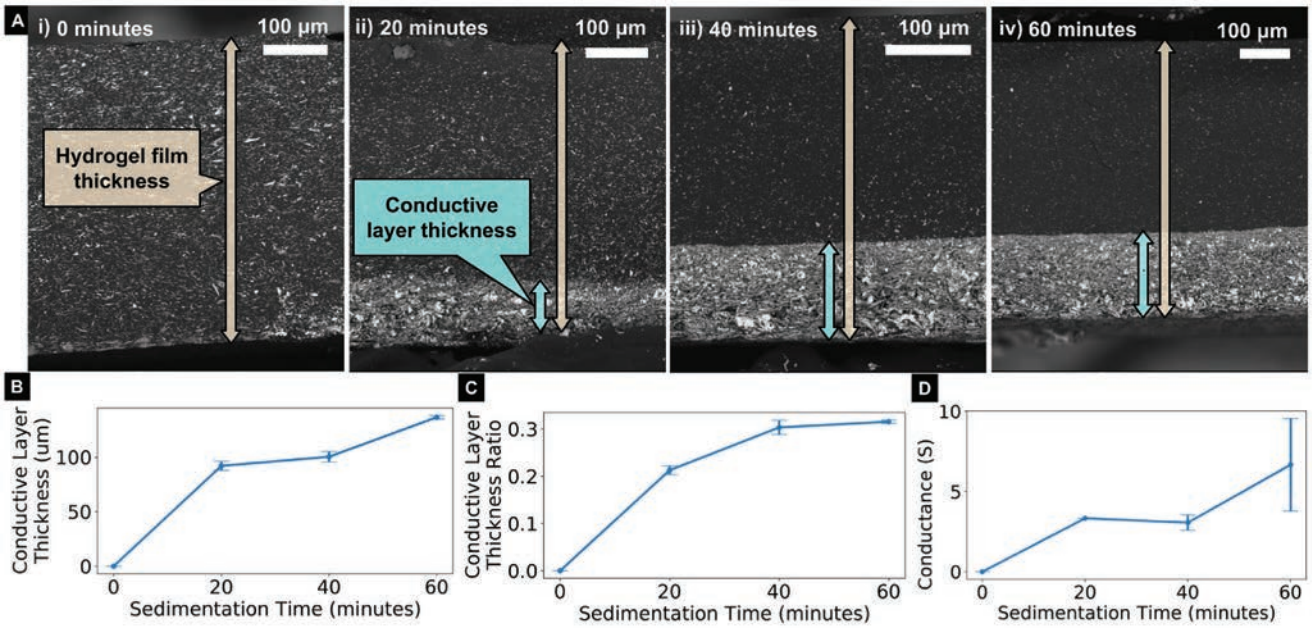

Figure 3. A) Scanning electron microscopy (SEM) of conductive gelatin composite with a sedimentation time of i) 0 min, ii) 20 min, iii) 40 min and iv) 60 min. B) Growth in thickness of the conductive layer as sedimentation time increases. C) Growth in relative thickness of conductive layer as sedimentation time increases. D) Increase in conductance of material samples as sedimentation time increases.

composition of coagulated gelatin (CG), glucose syrup, glycerol and water in a 1:1:1:12 weight ratio. From there, there are two variations in matrix composition. Pristine gelatin (PG) samples use a composition with unmodified gelatin powder in place of the coagulated gelatin, to explore the influence of the longer polymer chains induced by coagulation. Glycerol-rich gelatin (GG) samples use twice the amount of glycerol in order to examine its influence as a plasticizer and viscosity modifier for the molten state of the hydrogel. For all variations in the matrix composition, versions with silver flakes as conductive filler are also characterized separately (e.g., non-conductive pristine gelatin (PG-NC) versus conductive pristine gelatin (PG-C)). All of PG-C, CG-C, and GG-C achieved high electrical conductivity of over 10^2 S cm^{-1}.

In addition to the hydrogel composition, we also examine the influence of Ag flake settling and sedimentation. During the silver flake sedimentation step (**Figure 3**), the microstructure of the material transitions from uniformly dispersed and disconnected silver flakes to a bilayer structure of gelatin-rich and silver-rich layers. Within the sedimented Ag-rich layer, the silver flakes form a dense, percolating network that is electrically conductive (Figure 3A). The thickness of this layer grows throughout this process (Figure 3B,C), resulting in a lower electrical resistance on the sedimented side of the composite (Figure 3D). There appears to be a point in settling where the transition from the conductive layer to insulating layer is no longer a gradient of decreasing silver flake concentration and is instead a more discrete transition. This can cause delamination or fracture as shown in Figure S2 (Supporting Information). This mechanical failure mode can be avoided by controlling sedimentation time, and should have some dependency on molten matrix viscosity.

2.2. Materials Characterization

We examine the influence of material composition and processing conditions on the properties of the composite. These include mechanical characteristics (elastic modulus, elastic resilience, strain at break), electrical conductivity, and coupling between elastic strain and electrical resistivity.

2.2.1. Mechanical Properties

Figure 4A presented stress–strain curves under tensile loading for each hydrogel composition with and without Ag filler. As can be seen in the strain at break data extracted from these curves (Figure 4B) the conductive compositions generally exhibit lower elongation at failure (approximately 30–50% for CG-C and PG-C compared to approximately 85–185% for CG-NC and PG-NC). This is likely due to the conductive filler introducing microscale defects in the hydrogel matrix that initiate failure. We also observe that the GG samples generally exhibit the highest elongation at break. The excess glycerol present in these materials acts as an effective plasticizer and creates a much higher elongation before specimen failure, likely due to enhanced mobility of gelatin chains.[31] This effect appears to overwhelm the effect of adding conductive filler, since GG-C and GG-NC have greatly overlapping error bars and very similar mean strains at break (approximately 500% vs. 470%). Finally, it appears that the coagulation process enables larger elongation as well. Comparing CG-NC and PG-NC samples that have no conductive filler, they differ only in that CG-NC uses coagulated gelatin. There is little overlap in their error-bars, with CG-NC having a mean strain at break of 186%, compared to PG-NC with 87%. Coagulation creates longer polymer chains, providing the opportunity for more entanglements that can dissipate energy before bond-breaking.[29] Similar

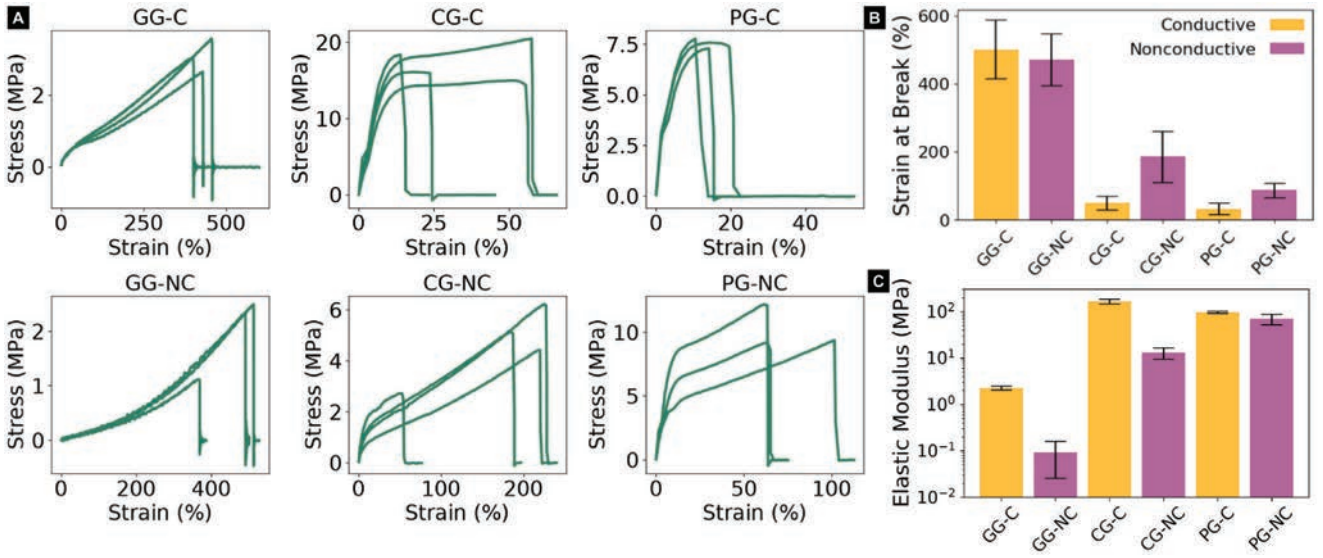

Figure 4. A) Stress–strain curves of tensile failure testing of different compositions of gelatin composite. B) Strain at break of these compositions. C) Elastic modulus of these compositions.

correlations exist when looking at the elastic modulus of the different compositions. As we can see in Figure 4C, the presence of conductive filler increases the stiffness of the gelatin hydrogel. This trade-off between high electrical conductivity and having a compliant mechanical properties appears to be alleviated both by using coagulated gelatin as the matrix polymer and especially by increasing the amount of glycerol plasticizer.

Mechanical hysteresis of different compositions under cyclical loading up to 10% strain is shown in **Figure** 5A. Three samples of each are overlaid, to demonstrate consistency within each composition. The first cycle, indicated visually by full saturation, shows a higher stress than subsequent cycles, consistent with stress-softening. Unfilled coagulated gelatin hydrogel with double glycerol GG-NC follows virtually the same path through stress-strain space after the first cycle, thus displaying minimal hysteresis. Filled coagulated gelatin hydrogel with double glycerol GG-C and unfilled coagulated gelatin hydrogel CG-NC have slightly higher hysteresis, while the filled coagulated gelatin hydrogel CG-C and both filled and unfilled pristine gelatin hydrogels PG-C and PG-NC demonstrate noticeable hysteresis. This is quantified by calculating the average resilience of each composition (Figure 5B) across three samples.

Elastic resilience for each sample is calculated by first offsetting the values so all stress values are positive, then summing the integrals of the loading stress from 0% to 10% strain for all cycles. This is the energy stored in the material throughout the cyclical process. A sum for the unloading cycles is obtained as well, representing the energy released during unloading. The ratio of the energy released to the energy stored $\frac{U_{r,unloading}}{U_{r,loading}}$ is reported as the resilience of the sample. Nonconductive, unfilled compositions demonstrate higher resilience than their filled counterparts

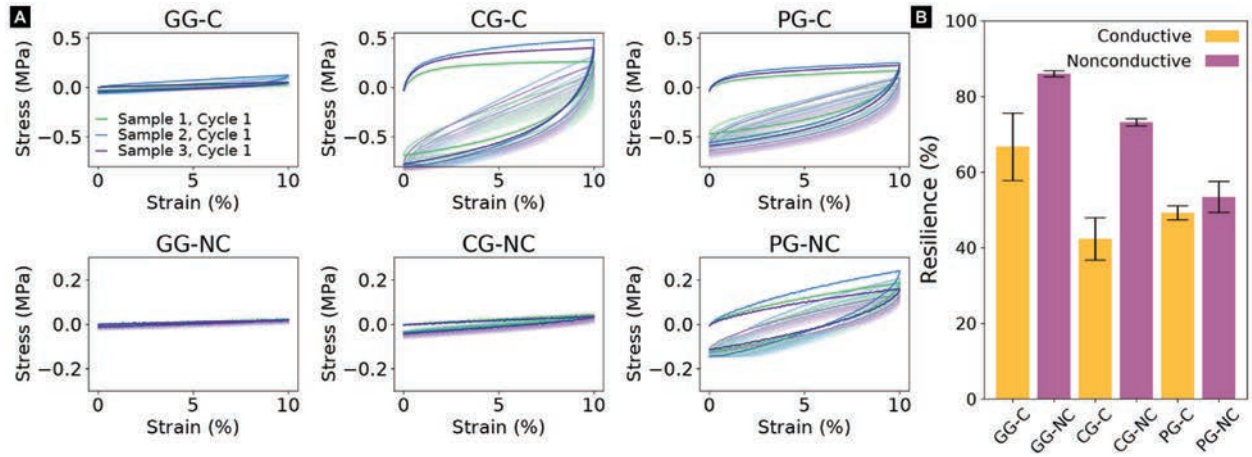

Figure 5. A) Hysteresis curves of different compositions of gelatin composite. Color saturation decreases and value increases for later cycles. B) Derived mechanical resilience of these compositions.

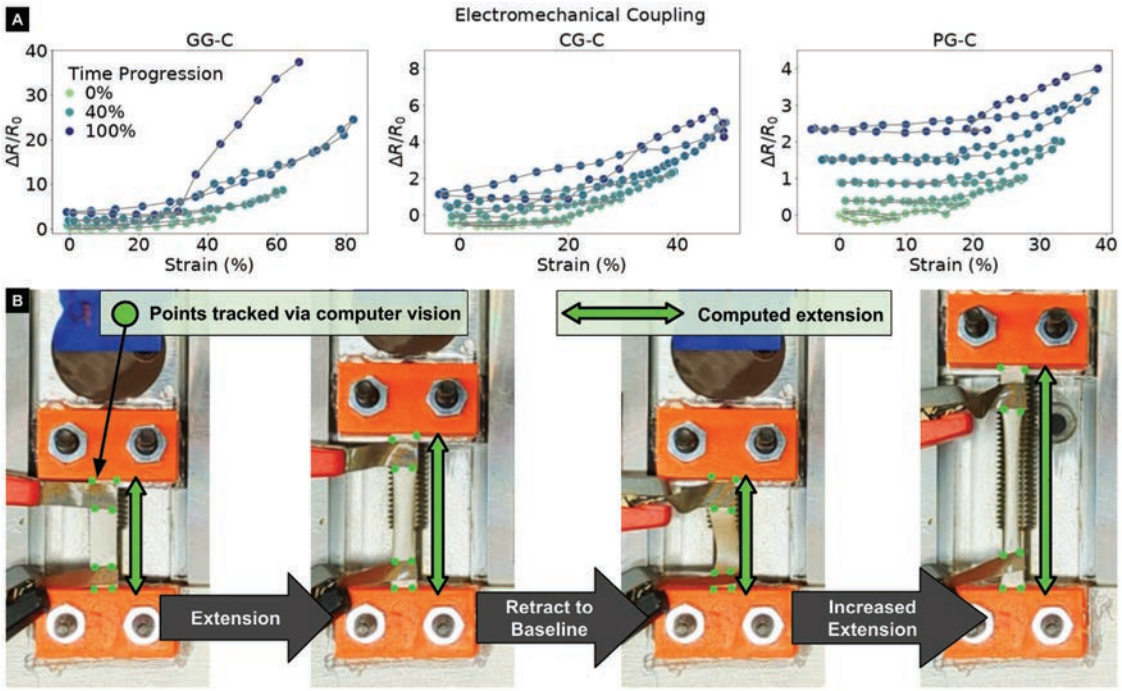

Figure 6. A) Relative resistance change as strain iteratively increases. B) Experimental setup for electromechanical testing.

across the board. This is expected due to plasticity induced by rearranging of filler particles during deformation. Unfilled pristine gelatin hydrogel PG-NC demonstrates noticeably less resilience than unfilled coagulated gelatin hydrogel CG-NC. This indicates that the longer polymer chains of coagulated gelatin are better at storing energy elastically than the shorter chains of unmodified gelatin. For the filled versions, CG-C and PG-C, the range of their resilience overlaps, likely because the presence of conductive filler dominates the differences in chain length. The highest resilience filled hydrogel is GG-C, due to the presence of double the amount of plasticizer.

2.2.2. Electromechanical Properties

Representative electromechanical response curves for GG-C, CG-C, and PG-C hydrogel compositions are shown in **Figure 6A**. These curves were collected from rectangular strips of material using the test rig shown in Figure 6B. All compositions demonstrate a coupling between the relative increase in resistance and applied strain. There is a hysteretic element to the increase in resistance as the samples are stretched to higher strains. There is a close alignment of the relaxation trajectory to the stretching trajectory of that cycle. This is an electrical analogue to the stress-softening of filled polymers (Mullins effect[32]), possibly due to changes to the arrangement of filler particles (Ag microflakes) when experiencing new maximum strain. This suggests that once stretched to some maximum, the electromechanical coupling would be more consistent within previously experienced strain ranges. Such electromechanical and cyclical behaviors are not unique to this composite and have been previously observed with other soft material systems that use silver as the conductive filler.[33]

We note that variations in electromechanical response exist even among samples of the same material composition, as shown in Figure S5 (Supporting Information). Such sample-to-sample variation is observed to coincide with differences in the tensile strain at electrical circuit failure. One explanation could be the stochastic nature of material defects within the composites, which manifest themselves in both electromechancial coupling and electrical failure. Aside from these variations, we observe that when comparing between compositions, CG-C and PG-C have similar curves and ultimate strains. GG-C follows a similar pattern, but goes to much higher ultimate strains. This follows due to the increased compliance added by having twice as much glycerol as the other compositions.

When considering the target applications of these hydrogels, the long term stability of the material is also important to understand. A preliminary study was conducted through IV characterization, water retention and resistance measurements of several GG-C samples over seven days following the dehydration step (Figure S6, Supporting Information). The IV characterization shows that the material behaves like a resistor according to Ohm's Law over the course of the seven days (Figure S6A, Supporting Information). During that time, the mass of the sample changes very little, suggesting that the dehydration step is effective at removing the leftover volatile components, which should help improve the stability of the gels over time (Figure S6B, Supporting Information). Finally, the resistance of the samples tended to decrease over the course of the seven days (Figure S6C, Supporting Information). There could be two main reasons for this given the lack of further mass loss in the other samples. The first reason this trend could be occurring is that the ends of the

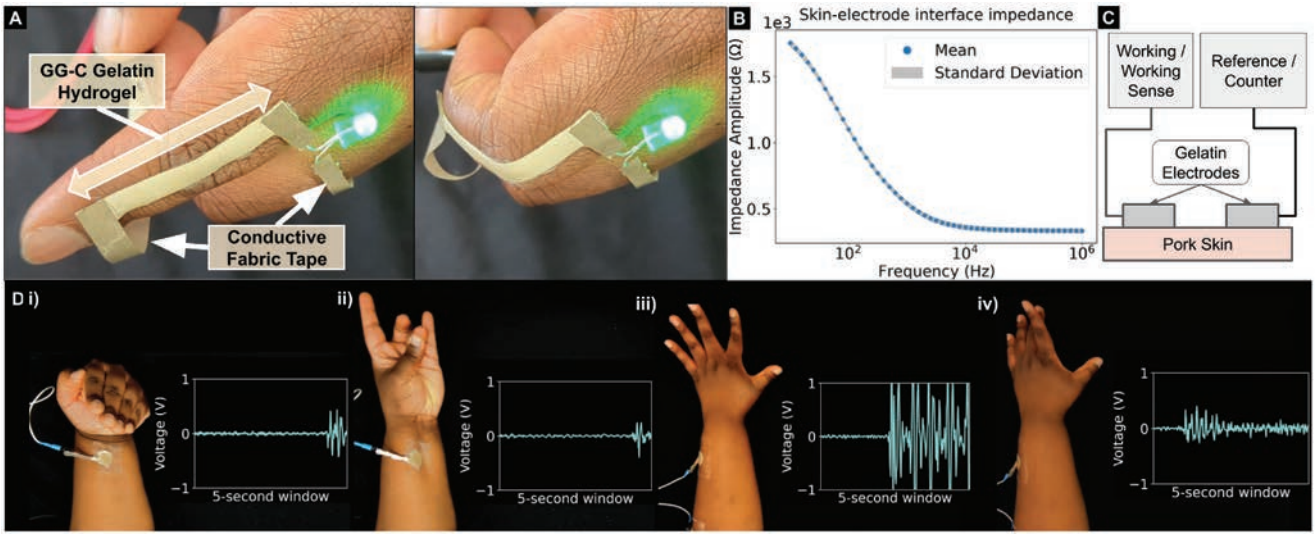

Figure 7. A) Demonstration of conductive gelatin sample conforming to hand during flexing while functioning as wire. B) Impedance curve of skin-electrode interface in pig-skin characterization experiment. C) Schematic diagram of impedance analysis setup with Gamry potentiostat. D) Electromyograms of muscle activity during 1) wrist flexion 2) ring-finger flexion 3) wrist and finger extension with rocking 4) finger extension, held till activity extinction.

samples were damaged during testing due to probe insertion, which forced the test leads to be inserted closer together, reducing the length of the samples over time and thus leading to a natural decrease in resistance according to Pouillet's Law. The second explanation for this phenomenon could be that further dehydration not captured in the water retention study occurred due to Joule heating of the samples, as a high amount of current passed through these samples during testing at higher voltages, which could lead to heat-based water evaporation that drove the conductivity lower. Despite these changes, the overall conclusions from these tests suggest that the gels are relatively stable due to the dehydration step.

2.3. Demonstrations

The mechanical and electrical properties of this conductive biopolymer composite suggest possible applications in soft and wearable electronics. Here, we present two representative cases in which the material can be placed on the skin and maintain electrical functionality during body motion.

To demonstrate applicability for soft wearable circuits, a rectangular strip of GG-C conductive hydrogel was mounted to the index finger and used for delivering electrical current to a 3-volt light-emitting diode (LED). Referring to **Figure** 7A, the strip adheres to the finger across the middle and proximal phalanx and remains functional through the full bending range of motion of index finger. Additionally, when detached from the skin, we show that the circuit remains functional under gravitational loading, tensile stretching, and twisting(Figure 1E, i–iii).

Furthermore, we demonstrate the ability to use the materials for electromyography (EMG). Generally speaking, electrodes for electrical biosignal recording need to be highly conductive and possesses conformal compliance, features which are present in this conductive gelatin hydrogel. For electromyography, an impedance response curve with sensitivity in the 100Hz to 10kHz range is needed, which is demonstrated by electrodes cut from GG-C composition (Figure 7B). This curve was obtained via testing on a pork skin model with a Gamry potentiostat in 2-lead mode (Figure 7C). The signals recorded from human muscle activation with attached gelatin electrodes are shown in Figure 7D. Electrodes are tested while placed over the flexor digitorum muscle (Figure 7D, i–ii) and the extensor digitorum muscle (Figure 7D, iii–iv). Recorded voltage traces are visually distinguishable from background, and demonstrate expected features including spikes at both activation and relaxation (Video S7, Supporting Information), continued activity under movement (Figure 7D, iii), and activity extinction while holding position (Figure 7D, iv).

3. Discussion and Conclusion

In this study, we examine the use of food-grade gelatin as a matrix material for soft electronics. Gelatin is attractive as a material for use in environmentally sustainable electronics because it can be sourced from agricultural waste. The close proximity of agricultural sources to large population centers is common due to the inherent demand of agricultural products. As policy-makers focus increasingly on climate resilience and short agricultural supply chains fall into greater focus, technology that leverages those sources and provides additional use for waste become increasingly appealing. It is also possible to establish a renewable source of a given biomaterial via the agricultural cultivation of its source organism, so long as an appropriate growing environment is available or can be created. Combined, these factors mean that biomaterial-based systems like the silver-gelatin composites introduced here have the potential to minimize the climate effects of future soft electronic technologies.

Accessibility to makers, hobbyists, low-resource educational/academic environments and small businesses is a design goal that complements and extends the existing sustainability benefits of biomaterial-based composites. By focusing on accessibility, it becomes possible for this technology to enter into public consciousness directly, without relying on policy change or profitability. Existing efforts in this direction, for example libraries of biomaterial recipes that are open to the public,[34] demonstrate demand for this kind of knowledge. Increasing the potential functionality of those materials (e.g., adding conductivity as is done in this work) reinforces their utility and potentially further increases appeal. Improving access to this technology provides an avenue for broadening education into biomaterial-based technologies, through the process of "citizen science".[35,36] This could have downstream improvements to the number of people who study and work in the field, and in improving popular support for sustainability policy that relies on an understanding of feasible alternatives to fossil-fuel material supply streams. Our conductive hydrogel composite is composed primarily of inexpensive food-grade materials and can be fabricated without expensive equipment, chemically hazardous reagents and restrictive fabrication processes, allowing this material system to be relatively accessible. By focusing on equipment and materials that are purchasable for consumer use cases, this work potentially lowers start-up and ongoing costs, enabling people with less capital to engage with production and study of these materials. By minimizing hazardous material use, people with less training can more easily participate in the creation of these materials.

The usage of silver microflakes provides an opportunity to further increase the sustainability and accessibility of the material system in future work. In a soft electronics context, silver is attractive due to its high conductivity and the relative availability of various form factors that are popular in a multitude of industrial and commercial applications.[37] There are challenges associated with their use as well. First, there are potential respiratory hazards involving breathing particles of this size, and proper ventilation practices during handling and preparation need to be taken, which is demonstrated in the Video S4 (Supporting Information). Research has shown that various morphologies of silver, if released into the environment, pose ecological risks. Ag nanoparticles have potentially useful antimicrobial effects,[38] but have been shown to negatively affect the health of fish[39] and aquatic invertebrates.[40] Due to the potential for mechanical or chemical conversion to nanoparticles or Ag ions after disposal, life cycle considerations must be made.

With advancements in engineering, science, and technology, researchers are looking for sustainable designs and approaches to minimize e-waste.[41–43] Tavakoli et al. demonstrated soft electronics that are resilient, repairable if damaged and recyclable.[44] Sanati et al. demonstrated the recovery of metals like silver and gallium from disposed supercapacitors through an electrowinning technique.[45] Carneiro et al. demonstrated that soft electronics made with silver flakes and polyurethane composites can be decomposed into polyurethane residue and reusable silver-rich powder via appropriate solvents (isopropyl alcohol (IPA)).[46] The gelatin-based composite shown in this work could be dissolved with water as an effective solvent instead of IPA. Reclaiming the silver flakes in this way could allow both recycling of material rather than inciting further resource extraction, as well as preventing the release of silver into aquatic environments. As future work, there is the potential to partially or completely obviate these issues with the use of more biocompatible conductive fillers like graphene oxide,[18,19,47] poly(3,4-ethylenedioxythiophene) polystyrene sulfonate (PEDOT:PS),[48,49] activated carbon,[50] zinc[4] or molybdenum,[51] and hopefully accessible fabrication methods using these options can be pursued in the future. The structural complexity of components or devices produced from these hydrogels also shows potential for further development, and hydrogel printing techniques[52] potentially provide an avenue to more complex devices fabricated from these biomaterial hydrogel composites.

4. Experimental Section

Materials: Hydrogel composite composed of the following: gelatin powder (300 Bloom Porcine, Superclear, Custom Collagen), glucose syrup (DE 45-49, Pastry 1) and glycerol (vegetable glycerin, SimpleNature). For conductive compositions, additionally used silver microflakes (99.9% pure, APS 2–5 microns, 47MR-10F, Inframat Advanced Materials) and concentrated dishwashing liquid (Ultra, Dawn). For coagulation of gelatin in CG and GG variants, isopropyl alcohol (Technical Grade 99%, R-615-1, PTI Process Chemicals) was used.

Hydrogel Fabrication—Gelatin Coagulation: The gelatin coagulation process is based on Stoessel et al.[53] as shown in Video S3 (Supporting Information). Distilled water (4 g/40 wt%) was mixed with isopropyl alcohol (5 g/50 wt%). Gelatin powder (1 g/10 wt%) was added to the solution. Due to the high solubility of gelatin in water and its low solubility in alcohol, a ternary solution with two phases is formed.[53] Vial with solution is placed in water bath, kept at 50° C using an induction cooktop (COS-YLIC1, Cosmo) and allowed to rest undisturbed for 5 min. After resting time, the solution was shaken by hand to agitate for 30 s. This cycle of resting and agitation Was repeated for 30 min, increasing the length of gelatin chains over time. Afterwards, the supernatant phase was decanted, leaving behind a dope phase composed of coagulated gelatin and residual absorbed water/isopropyl for use in hydrogel synthesis.

Hydrogel Fabrication—Silver Flake Preparation: Silver microflakes were prepared under fume hood ventilation as shown in Video S4 (Supporting Information). Distilled water (3 g) was mixed with concentrated dishwashing liquid (0.2 g) as a surfactant in a scintillation vial to produce a soapy solution. Silver microflakes (3 g) were dispersed in soapy solution and shaken to ensure all flakes were wetted to prevent aerosolization during subsequent hydrogel synthesis, as well as to prevent inappropriate accumulation of silver flakes due to surface tension.

Hydrogel Fabrication—Hydrogel Synthesis: Hydrogel composites were prepared according to process shown in Video S2 (Supporting Information). For PG-C composition, in a scintillation vial glucose syrup (1 g) was mixed with glycerol (1 g), distilled water (9 g) and a suspension of silver filler particles (3.2 g soapy solution, 3 g silver microflakes). Mixture was heated in a water bath to 50°C to lower the viscosity of the glucose syrup, then agitated by hand to mix. Gelatin powder was slowly added to allow granules to hydrate without clumping, producing a 1:1:1:12 weight ratio of gelatin powder, glycerol, glucose syrup and water. Once all gelatin powder was hydrated, the sealed vial was placed in a water bath at 80° C for 1 h, until molten. For CG-C composition, coagulated gelatin (1 g, plus absorbed water and isopropyl alcohol) was added instead of gelatin powder, producing a 1:1:1:12 weight ratio of coagulated gelatin, glycerol, glucose syrup, and water. For GG-C composition, coagulated gelatin (1 g, plus absorbed water and isopropyl alcohol) was also used, and an additional 1 g of glycerol was added, producing a 1:2:1:12 weight ratio of coagulated gelatin, glycerol, glucose syrup and water. PG-NC, CG-NC and GG-NC nonconducting variants were synthesized similarly to their respective conductive counterparts by replacing the silver microflake suspension with distilled water (3 grams), and then skipping the subsequent sedimentation step.

Larger sheets of material were produced by multiplying ingredient quantities; sheets used for consistent comparison in this work were fabricated with 16x the reference quantities and poured onto aluminum or silicone sheets to cast (Figure S3, Supporting Information). At this stage, the silver content was 5.4 vol%.

Hydrogel Fabrication—Silver Flake Sedimentation: Silver flakes were assembled into a conducting layer via sedimentation in the molten hydrogel matrix. Hydrogel was kept above its composition-dependent melting point of around 85° C via double-boiler method over an induction cooktop (COS-YLIC1, Cosmo) as shown in Video S2 (Supporting Information). Due to presence of surfactant, flakes do not remain floating on the top surface, and all microflakes sink over time under force of gravity due to higher filler density than matrix density. This process is illustrated in Figure 2C and Figure 3A. Hydrogel was kept in this molten state for 1 h, then allowed to cool, resulting in sheets of conductive hydrogel composite. The microstructure of different compositions can be seen in Figure S1 (Supporting Information).

Hydrogel Fabrication—Hydrogel Dehydration: After hydrogel samples cool down enough to gel, they were dehydrated for 48 h in a food dehydrator (CP267-FD, Cosori) at 35° C, kept below 10% humidity as tracked by a humidity monitor (1731, Taylor) inside the dehydration chamber. Excess water was driven off, with stable amounts retained by the humectant properties of glycerol. If all water is removed, the silver fraction rised to 18.3 vol%.

Material Characterization—Electrical Characterization: Conductivity measurements were performed using a digital multimeter (Fluke 177 True-RMS Digital Multimeter, Fluke) in 2-probe mode. Contact resistance between probe and material was reduced by immersion in droplets of gallium-based liquid metal, produced in house from 75% Gallium (99.99%, Rotometals) and 25% Indium (99.99% Rotometals). Rectangular strips of conductive hydrogel material are cut from sheets and dimensions are measured using digital calipers (6 in. 3-Mode Digital Fractional Caliper, Husky), three times for each dimension with median measurement used. Conductivity calculated according to $\sigma = \frac{l}{R*w*h}$, where R is resistance in Ohms across the strip, minus contact resistance, and l, w, h are the length, width and thickness of the sample.

Additional analysis was completed to determine that the liquid metal interconnects were sufficient in reducing contact resistances necessary for measurement. Three samples of size 3 cm by 1 cm (length by width) were cut from a sheet of GG-C hydrogel. The resistance of each sample was measured using a digital multimeter in 2-probe mode (Fluke 177 True-RMS Digital Multimeter, Fluke) and in 4-probe mode (Keithley 2100 6 1/2 Digital Multimeter, Keithley) with and without liquid metal. The comparison data is provided in Table S1 (Supporting Information).

Material Characterization—Tensile Failure: Data for strain-at-break and elastic modulus presented in Figure 4B, 4C was collected via a materials universal testing machine (5969, Instron) with a 50N load cell (2530-50N, Instron). Samples of composite were prepared as dogbone coupons (Die C, 1/2 scale, ASTM D412) and secured with manual wedge action grips (2716-016, Instron). Samples were strained at 3 mm min^{-1} rate until failure. Experiments were repeated 3-4 times per composition.

Material Characterization—Mechanical Hysteresis: Mechanical hysteresis measurements were taken using materials universal testing machine (5969, Instron) with 50N load cell (2530-50N, Instron). Samples of composite were prepared as dogbone coupons (Die C, 1/2 scale, ASTM D412) and secured with manual wedge action grips (2716-016, Instron). A strain curve was programmed at 10 repetitions, with 5 mm min^{-1} strain rate and 0–10% strain range. All samples experienced slack removal via pre-stress of less than 1N. Experiments were repeated 3 times per composition.

Material Characterization—Electromechanical Characterization: Electromechanical characterization was performed on the setup as shown in Figure 6B. Rectangular coupons of conductive hydrogel composite were cut from a sheet and dimensions were recorded for strain normalization. Coupon is clamped to manual linear stage (Unislide A25 Series, Velmex) using textured clamping blocks printed on a fused deposition 3D printer (MK3S, Prusa) from PLA (Prusament, Prusa). Double sided silver conductive tape (Gray-T-C-25-20, JUFU) was bonded to the coupon at both ends using silver epoxy (8331D, MG Chemicals), and probes were clamped to this tape to connect to a digital multimeter (34401A, Agilent) for continuous monitoring. During testing (shown in Video S5, Supporting Information), coupon was stretched by hand-cranking the linear stage, then returning it to the initial position. Each cycle, the amount stretched Was increased by one revolution for PG-C and CG-C and two revolutions for GG-C (0.1 inches advanced per revolution). Test was monitored optically by video recording using an overhead mounted smartphone camera (Pixel 6, Google). Bounding boxes were selected around visual intersection of the coupon and clamping block, and strain over time is calculated using computer vision box-tracking with OpenCV Python library.

Material Characterization—Long Term Stability Characterization: GG-C samples were fabricated and subjected to an additional long term stability characterization. The summary of the experiments is shown in Figure S6 (Supporting Information). Six total samples (three for IV and resistance characterization, three for water retention test) of size 3cm x 1cm were cut from a bulk sample. All tests were conducted over seven days of monitoring in an open air lab environment around 23° C and a relative humidity of 42%, with "Day 0" representing the values of the samples immediately after the dehydration step. Readings were taken at every 24 h interval.

Three of these samples underwent IV characterization through the use of a power supply (SPS305, Kungber)—for a given input voltage (discrete values of 0–1.5V inclusive, with 0.25V increments), the corresponding current was measured from the power supply readout (Figure S6A, Supporting Information). Liquid metal was used to reduce the contact resistance between the power supply and the samples. A linear fit was performed to compare the experimental data to Ohm's Law.

Three different samples were used to perform a water retention test. Different samples were chosen from the samples used for the IV characterization test due to the concern of potential damage from testing and the added weight of the liquid metal, which could have potentially skewed results. These new samples were measured on a scale (HR-250AZ, A&D Company, Limited) and normalized by their starting mass. The normalized masses were then averaged together for each day to produce a mean and standard deviation (Figure S6B, Supporting Information).

Using Ohm's Law ($R = \frac{V}{I}$) and the data/samples from Figure S6A (Supporting Information), the resistances for each sample at each voltage were calculated. These resistances were then averaged across each sample and normalized to its initial average resistance immediately after dehydration. Finally, an average and standard deviation across the three samples were taken for each day (Figure S6C, Supporting Information).

Material Characterization—Scanning Electron Microscopy (SEM): Scanning electron micrscope images collected from samples after 48 h-dehydration, using a benchtop scanning electron microscope (PW-100-018, Phenom XL, Phenom). Settings for the microscope were 10kV beam strength with 0.1 Pa vacuum pressure.

Material Characterization—Fourier Transform Infrared Spectroscopy: To collect data in Supplemental Information Figure S7 (Supporting Information), a Fourier transform infrared spectrometer (Frontier FTIR Spectrometer, PerkinElmer) was used in conjunction with platinum ATR single-reflection diamond accessory (sample scans, 64; resolution, 4 cm^{-1}).

Demonstrations—Wearable Soft Circuit: A soft circuit was constructed with an LED (20mA,3-3.2V, 60F5W-YT-6SE-6SE, CHANZON) as the load. LED was connected to double sided silver conductive tape (Gray-T-C-25-20, JUFU) using silver epoxy (8331D, MG Chemicals), which is then epoxied to conductive hydrogel composite GG-C. Hydrogel composite is placed across index finger joint as shown in Figure 7A, or wrist joint as shown in Video S6 (Supporting Information), conformally attached using a medical transfer adhesive (1524A, 3M). Joint was flexed repeatedly while current is carried through conductive composite, demonstrating a stable percolating network. An informed written consent was obtained from the participant. As the demonstration was only performed on the first author of this manuscript, this study did not receive full IRB review.

Demonstrations—Impedance Characterization: Electrodes were cut from conductive hydrogel sheet (GG-C) using a 10cm diameter stencil. Electrodes were attached conformally to the pork skin substrate with tape

(539H, 3M), and connected to a potentiostat (Interface 1000, Gamry) in 2-probe mode as shown in Figure 7C. Electrodes placement distance is 1.5x the electrode diameter of 10cm. Impedance curve was measured 10 times to produce the mean and standard deviation curves shown in Figure 7B,

Demonstrations—Electromyography electrodes: Two conductive hydrogel electrodes were placed across relevant muscle groups, extensor digitorum for extension and flexor digitorum for flexion, with placement derived from Atlas of Muscle Innervation Zones.[54] Electrodes were attached conformally using medical transfer adhesive (1524A, 3M). Disposable self-adhesive clinical grade electrodes (HEX Dual Electrodes #272S, Noraxon) were used as reference electrodes, placed near the olecranon prominence of the elbow (electrodes shown in Figure S4, Supporting Information). Both the hydrogel electrodes and reference electrodes were connected to an open source biosensing board (Cyton V3, OpenBCI), which communicates to a neighbor computer through a wireless USB receiver. During demonstration, activity from finger and wrist motion is recorded through hydrogel electrodes as shown in Figure 7D and Video S7 (Supporting Information). Recorded data was filtered using a Butterworth bandpass filter from 5–50Hz followed by notch filter at 50Hz and 60Hz. An informed written consent was obtained from the participant. As the demonstration was only performed on the first author of this manuscript, this study did not receive full IRB review.

Supporting Information

Supporting Information is available from the Wiley Online Library or from the author.

Acknowledgements

The authors acknowledge use of the Materials Characterization Facility at Carnegie Mellon University supported by grant MCF-677785. The authors acknowledge support from the National Science Foundation Graduate Research Fellowship Program (GRFP) and the Carnegie Mellon University Robotics Institute.

Conflict of Interest

The authors declare no financial or commercial conflicts of interest.

Data Availability Statement

The data that support the findings of this study are available from the corresponding author upon reasonable request.

Keywords

biomaterials, conductive composites, gelatin, hydrogels, soft electronics

Received: July 25, 2024
Revised: December 9, 2024
Published online:

[1] E. Kabir, R. Kaur, J. Lee, K.-H. Kim, E. E. Kwon, *J. Cleaner Prod.* **2020**, *258*, 120536.
[2] R. G. Fonseca, A. Hajalilou, M. Freitas, A. Kuster, E. Parvini, A. C. Serra, J. F. Coelho, A. C. Fonseca, M. Tavakoli, *Adv. Mater. Technol.* **2023**, 2301007.
[3] D. Luo, A. Maheshwari, A. Danielescu, J. Li, Y. Yang, Y. Tao, L. Sun, D. K. Patel, G. Wang, S. Yang, T. Zhang, L. Yao, *Nature* **2023**, *614*, 463.
[4] S. Dahal, W. Yilma, Y. Sui, M. Atreya, S. Bryan, V. Davis, G. L. Whiting, R. Khosla, *Sensors* **2020**, *20*, 6154.
[5] C. V. Toniciolli Rigueto, M. Rosseto, I. Alessandretti, R. de Oliveira, D. A. R. Wohlmuth, J. Ferreira Menezes, R. A. Loss, A. Dettmer, I. R. Pizzutti, *Food Research Int.* **2022**, *162*, 112114.
[6] X. Wang, Z. Bai, M. Zheng, O. Yue, M. Hou, B. Cui, R. Su, C. Wei, X. Liu, *J. Sci.: Adv. Mater. Dev.* **2022**.
[7] C. Fletcher, W. J. Ripple, T. Newsome, P. Barnard, K. Beamer, A. Behl, J. Bowen, M. Cooney, E. Crist, C. Field, K. Hiser, D. M. Karl, D. A. King, M. E. Mann, D. P. McGregor, C. Mora, N. Oreskes, M. Wilson, *PNAS Nexus* **2024**, *3*, e106.
[8] F. Hartmann, M. Baumgartner, M. Kaltenbrunner, F. Hartmann, M. Baumgartner, M. Kaltenbrunner, *Adv. Mater.* **2021**, *33*, 2004413.
[9] F. Mushtaq, Z. A. Raza, S. R. Batool, M. Zahid, O. C. Onder, A. Rafique, M. A. Nazeer, *Int. J. Biol. Macromol.* **2022**, *218*, 601.
[10] J. Wang, M.-F. Lin, S. Park, P. S. Lee, *Mater. Today* **2018**, *21*, 50.
[11] M. Baumgartner, F. Hartmann, M. Drack, D. Preninger, D. Wirthl, R. Gerstmayr, L. Lehner, G. Mao, R. Pruckner, S. Demchyshyn, L. Reiter, M. Strobel, T. Stockinger, D. Schiller, S. Kimeswenger, F. Greibich, G. Buchberger, E. Bradt, S. Hild, S. Bauer, M. Kaltenbrunner, *Nat. Mater. 2020 19:10* **2020**, *19*, 1102.
[12] A. Heiden, D. Preninger, L. Lehner, M. Baumgartner, M. Drack, E. Woritzka, D. Schiller, R. Gerstmayr, F. Hartmann, M. Kaltenbrunner, *Sci. Rob.* **2022**, *7*.
[13] J. Shintake, H. Sonar, E. Piskarev, J. Paik, D. Floreano, *IEEE International Conference on Intelligent Robots and Systems* **2017**, 6221.
[14] S. J. Matonis, B. Zhuang, A. F. Bishop, D. A. Naik, Z. Temel, C. J. Bettinger, *ACS Appl. Polym. Mater* **2023**, *5*, 6288.
[15] D. Hardman, T. G. Thuruthel, F. Iida, *NPG Asia Mater.* **2022**.
[16] X. Jing, X.-Y. Wang, H.-Y. Mi, L.-S. Turng, *Mater. Lett.* **2019**, *237*, 53.
[17] C. Liu, H. J. Zhang, X. You, K. Cui, X. Wang, *Adv. Electron. Mater.* **2020**, *6*, 2000040.
[18] J. Park, J. Jeon, B. Kim, M. S. Lee, S. Park, J. Lim, J. Yi, H. Lee, H. S. Yang, J. Y. Lee, *Adv. Funct. Mater.* **2020**, *30*, 2003759.
[19] K. Han, Q. Bai, W. Wu, N. Sun, N. Cui, T. Lu, *Int. J. Biol. Macromol.* **2021**, *183*, 2142.
[20] K. Chen, Y. Hu, M. Liu, F. Wang, P. Liu, Y. Yu, Q. Feng, X. Xiao, *Macromol. Mater. Eng.* **2021**, *306*.
[21] Y. Ohm, C. Pan, M. J. Ford, X. Huang, J. Liao, C. Majidi, *Nat. Electron.* **2021**, *4*, 185.
[22] Y. Zhao, Y. Ohm, J. Liao, Y. Luo, H.-Y. Cheng, P. Won, P. Roberts, M. R. Carneiro, M. F. Islam, J. H. Ahn, L. M. Walker, C. Majidi, *Nat. Electron.* **2023**, *6*, 206.
[23] M. J. Ford, D. K. Patel, C. Pan, S. Bergbreiter, C. Majidi, *Adv. Mater.* **2020**, *32*, 2002929.
[24] T. Gan, Q. Xiao, S. Handschuh-Wang, X. Huang, H. Wang, X. Deng, S. Hu, B. Wang, Q. Wu, X. Zhou, *ACS Appl. Mater. Interfaces* **2022**, *14*, 42744.
[25] C. A. G. Quispe, C. J. R. Coronado, J. A. Carvalho, *Renewable Sustainable Energy Rev.* **2013**.
[26] K. R. Siegel, K. McKeever Bullard, G. Imperatore, H. S. Kahn, A. D. Stein, M. K. Ali, K. M. Narayan, *JAMA Internal Medicine* **2016**, *176*, 1124.
[27] S. Shimizu, N. Matubayasi, *J. Phys. Chem. B* **2014**, *118*, 13210.
[28] E. S. Lazaro Vasquez, M. Alistar, L. Devendorf, M. L. Rivera, in, *Proceedings of the CHI Conference on Human Factors in Computing Systems*, CHI '24. Association for Computing Machinery, New York, NY, USA, ISBN 9798400703300, **2024**, pp. 1–18.
[29] J. Kim, G. Zhang, M. Shi, Z. Suo, *Science* **2021**, *374*, 212.
[30] C. Norioka, Y. Inamoto, C. Hajime, A. Kawamura, T. Miyata, *NPG Asia Mater.* **2021**, *13*, 1.

[31] M. W. M. Tan, P. M. Thornton, G. Thangavel, H. Bark, R. Dauskardt, P. S. Lee, *Adv. Sci.* **2024**.
[32] J. Diani, B. Fayolle, P. Gilormini, *Eur. Polym. J.* **2009**, *45*, 601.
[33] M. Tavakoli, M. H. Malakooti, H. Paisana, Y. Ohm, D. Green Marques, P. Alhais Lopes, A. P. Piedade, A. T. de Almeida, C. Majidi, *Adv. Mater.* **2018**, *30*, 1801852.
[34] Materiom, https://commons.materiom.org/materials-database, (accessed: June 2024).
[35] R. Bonney, C. B. Cooper, J. Dickinson, S. Kelling, T. Phillips, K. V. Rosenberg, J. Shirk, *BioScience* **2009**, *59*, 977.
[36] R. Bonney, T. B. Phillips, H. L. Ballard, J. W. Enck, *Public Understanding of Science* **2016**, *25*, 2.
[37] S. Temizel-Sekeryan, A. L. Hicks, *Resour. Conserv. Recycl.* **2020**, *156*, 104676.
[38] M. Do, L. Linhares, R. Menezes, N. Da, R. Pires, L. R. D. Cunha, M. D. F. Rosa, B. Warlene, S. D. Souza, J. P. D. A. Feitosa, M. De, S. M. D. S. Filho, *Food Packaging and Shelf Life* **2018**.
[39] J. M. Lacave, U. Vicario-Parés, E. Bilbao, D. Gilliland, F. Mura, L. Dini, M. P. Cajaraville, A. Orbea, *Sci. Total Environ.* **2018**, *642*, 1209.
[40] A. Magesky, É. Pelletier, *Cytotoxicity and Physiological Effects of Silver Nanoparticles on Marine Invertebrates*, Springer International Publishing, Cham, ISBN 978-3-319-72041-8, **2018**, pp. 285–309.
[41] M. Irimia-Vladu, *Chem. Soc. Rev.* **2014**, *43*, 588.
[42] D. K. Patel, K. Zhong, H. Xu, M. F. Islam, L. Yao, *Adv. Mater. Technol.* **2023**, *8*, 2300678.
[43] T. Cheng, T. Tabb, J. W. Park, E. M. Gallo, A. Maheshwari, G. D. Abowd, H. Oh, A. Danielescu, in *Proceedings of the 2023 CHI Conference on Human Factors in Computing Systems*, CHI '23. Association for Computing Machinery, New York, NY, USA, ISBN 9781450394215, **2023**.
[44] M. Tavakoli, P. Alhais Lopes, A. Hajalilou, A. F. Silva, M. Reis Carneiro, J. Carvalheiro, J. Marques Pereira, A. T. de Almeida, *Adv. Mater.* **2022**, *34*, 2203266.
[45] A. L. Sanati, P. Alhais Lopes, A. Chambel, A. F. Silva, D. M. Oliveira, C. Majidi, A. T. de Almeida, M. Tavakoli, *Chem. Eng. J.* **2024**, *479*, 147894.
[46] M. Reis Carneiro, A. T. de Almeida, M. Tavakoli, C. Majidi, *Adv. Sci.* **2023**, *10*, 2301673.
[47] J. Khan, M. Mariatti, *J. Cleaner Prod.* **2022**, *376*, 134254.
[48] H. He, L. Zhang, X. Guan, H. Cheng, X. Liu, S. Yu, J. Wei, J. Ouyang, *ACS Appl. Mater. Interfaces* **2019**, *11*, 26185.
[49] B. Lu, H. Yuk, S. Lin, N. Jian, K. Qu, J. Xu, X. Zhao, *Nat. Commun.* **2019**.
[50] L. Lamanna, G. Pace, I. K. Ilic, P. Cataldi, F. Viola, M. Friuli, V. Galli, C. Demitri, M. Caironi, *Nano Energy* **2023**, *108*, 108168.
[51] A. G. Kurian, N. Mandakhbayar, R. K. Singh, J.-H. Lee, H.-W. Kim, *ACS Appl. Mater. Interfaces* **2024**.
[52] W. Sun, J. W. Tashman, D. J. Shiwarski, A. W. Feinberg, V. A. Webster-Wood, *ACS Biomaterials Science and Engineering* **2022**, *8*, 303.
[53] P. R. Stoessel, R. N. Grass, A. Sànchez-Ferrer, R. Fuhrer, T. Schweizer, R. Mezzenga, W. J. Stark, *Adv. Funct. Mater.* **2014**, *24*, 1831.
[54] M. Barbero, R. Merletti, A. Rainoldi, *Atlas of Muscle Innervation Zones* **2012**.